Hindawi
Advances in Civil Engineering
Volume 2019, Article ID 6814367, 17 pages
https://doi.org/10.1155/2019/6814367

*Research Article*

# A New Efficient Modified First-Order Shear Model for Static Bending and Vibration Behaviors of Two-Layer Composite Plate

**Vu H. Nam,[1,2] Nguyen H. Nam,[3] Pham V. Vinh,[4] Dang N. Khoa,[5] Do V. Thom,[1] and Phung V. Minh[4]**

[1]*Division of Computational Mathematics and Engineering, Institute for Computational Science, Ton Duc Thang University, Ho Chi Minh City, Vietnam*
[2]*Faculty of Civil Engineering, Ton Duc Thang University, Ho Chi Minh City, Vietnam*
[3]*Faculty of Mechanical, Electrical, Electronic and Automotive Engineering, Nguyen Tat Thanh University, Ho Chi Minh City, Vietnam*
[4]*Department of Mechanics, Le Quy Don Technical University, Hanoi, Vietnam*
[5]*Department of Electrical and Electronics Technology, HCM City University of Food Industry, Ho Chi Minh City, Vietnam*

Correspondence should be addressed to Nguyen H. Nam; namnguyen822003@yahoo.com and Do V. Thom; thom.dovan.mta@gmail.com

Received 30 October 2018; Revised 26 December 2018; Accepted 14 January 2019; Published 13 March 2019

Academic Editor: Michael Yam



A two-layer (connected by stubs) partial composite plate is a structure with outstanding advantages which can be widely applied in many fields of engineering such as construction, transportation, and mechanical. However, studies are scarce in the past to investigate this type of structure. This paper is based on the new modified first-order shear deformation plate theory and finite element method to develop a new four-node plate element with nine degrees of freedom per node for static bending and vibration analysis of the two-layer composite plate. The numerical results are compared to published data for some special cases. The effects of some parameters such as the boundary condition, stiffness of the connector stub, height-to-width ratio, thickness-to-thickness ratio between two layers, and aspect ratio are also performed to investigate new numerical results of static bending and free vibration responses of this structure.

## 1. Introduction

Two-layer beam and plate are among the most commonly used structures in many fields of engineering, such as construction, transportation, and mechanical, because of their advantages in comparison with one-layer structures; we can see these structures in practice such as steel-concrete composite beams and plates, layered wooden beams and plates, and wood-concrete and timber-steel floor structures. Some advantages of this type of composite structure can be considered such as easy manufacturing, taking advantage of the material properties of two components which made the structure. In fact, there are many different grafting methods to manufacture two-layer beams or plates; for example, two components of a structure are sandwiched together at the edges, using glue or connector stub to bond two parts at the contact surface. Because of these advantages, many researchers have focused on the mechanical analysis of these structures.

Two-layer beam has been investigated by Foraboschi [1, 2] using an analytical method. Kryžanowski et al. [3] developed an analytical method to evaluate exact critical forces of two-layer composite columns. Grognec et al. [4] used the Timoshenko beam model for buckling analysis of two-layer composite beams with partial interaction. He and Yang [5, 6] presented the finite element method and higher order beam theory for buckling and dynamic problem of the two-layer composite beam. He et al. [7] carried out an analytical solution for free vibration and buckling of two- and three-layer composite beams based on a higher order beam theory. Hozan et al. [8] analyzed a two-layer composite planar beam with exact geometric and material nonlinearities as well as the finite slip between the layers.

Wu and coworkers [9, 10] used the 2D elasticity solution for analysis of two-layer beams with the viscoelastic interlayer and arbitrarily shaped interface. Large deformation analysis of two-layer composite beams was studied [11]. Based on the higher order beam theory and analytical model, Wen et al. [12] investigated the flexural response of the two-layer composite beam. Do et al. [13] presented static bending analysis of three-layer beams made of functionally graded materials in the thermal environment based on FEM and Mindlin theory. Cas et al. [14] used an analytical method to investigate the mechanical behavior of two-layer composite beams with interlayer slips. Ke et al. [15] used experimental and numerical FE methods to study local web buckling of single-coped beam connections with the slender web.

Latham et al. [16] developed a new finite element based on a new plate theory due to the Reissner plate theory for static bending of two-layer plates. Foraboschi and colleagues [17, 18] used an analytical model and experimental method for static bending of laminated glass plates. Layered plate with discontinuous connection was investigated by Foraboschi [19] using the exact mathematical model replacing discontinuous connections with a fictitious continuous medium. Foraboschi [20, 21] also detailed the mechanical behavior of three-layer plates using the exact mathematical model and elasticity solution. Wu et al. [22] applied the 3D exact solution to explore the two-layer plate bonded by a viscoelastic interlayer. Vidal et al. [23] presented a new approach to study the deflection and stress of the multilayer composite plate. Alinia et al. [24] applied the numerical nonlinear finite element method and theoretical p-Ritz energy method to analyze inelastic buckling and post-buckling behaviors of stocky plates under combined shear and in-plane bending stresses.

This paper aims to use the finite element method (FEM) based on a new modified first-order shear deformation plate theory (FSDT) to analyze static bending and free vibration of the two-layer composite plate. The proposed method shows the simple formulations and computational efficiency. The accuracy and reliability of the proposed method are validated with other published results. Several numerical examples and influence of some parameters on static bending and free vibration of the two-layer composite plate are also investigated; these new results have significant impacts on the use of this structure in practice.

The organization of this paper is as follows: Section 2 presents the finite formulation of static bending and free vibration of the two-layer composite plate based on a new modified first-order shear deformation plate theory. New numerical results for bending and free vibration analysis of these plates are computed and discussed in Section 3. Some major conclusions are given in Section 4.

## 2. Geometry and Theoretical Formulation

*2.1. Geometry and Assumptions.* The geometry model of the problem is a two-layer plate including two isotropic plates which bonded together at the contact surface using connector stubs, as shown in Figure 1. Two parts are of the same size in the $x-y$ plane with thickness $h_m$ for the bottom layer and $h_n$ for the top layer. To avoid the repetition of similar equations for the bottom layer and top layer, we use the subscript $m$ for the bottom layer, subscript $n$ for the top layer, and subscript st for the connector stub.

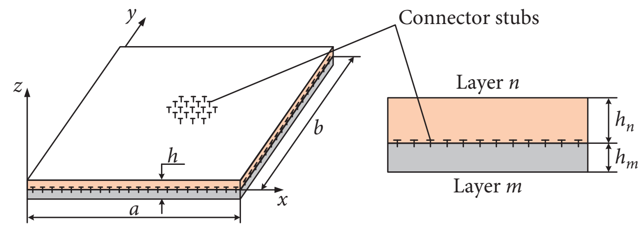


Figure 1: Geometrical notation of the two-layer plate.

The assumptions of the two-layer composite plate include the following: the materials of each layer are linear, elastic, and isotropic; the displacement and rotation of the plate are small; there is no delamination phenomenon between two layers; the deflection of the stub is in the contact interface of two components; and the mass of the stub is much smaller than the mass of the plate, so we assume that it is neglected.

*2.2. Discrete Finite Element Equations*

*2.2.1. New Modified First-Order Shear Deformation for Plate Elements.* The basic equations of the Mindlin plate theory are [25]

$$\begin{aligned}
M_x &= D\left(\frac{\partial\psi_x}{\partial x} + \nu\frac{\partial\psi_y}{\partial y}\right),\\
M_y &= D\left(\frac{\partial\psi_x}{\partial y} + \nu\frac{\partial\psi_y}{\partial x}\right),\\
M_{xy} = M_{yx} &= \frac{1}{2}(1-\nu)D\left(\frac{\partial\psi_x}{\partial y} + \frac{\partial\psi_y}{\partial x}\right),\\
Q_x &= S\left(\frac{\partial w}{\partial x} + \psi_x\right),\\
Q_y &= S\left(\frac{\partial w}{\partial y} + \psi_y\right),
\end{aligned} \tag{1}$$

where

$$\begin{aligned}
D &= \frac{Eh^3}{12(1-\nu^2)},\\
S &= kGh,\\
G &= \frac{E}{2(1+\nu)},
\end{aligned} \tag{2}$$

in which $k = 5/6$ is the shear correction.

Equilibrium of moments about $x$- and $y$-axis and transverse force leads to

$$\frac{\partial M_x}{\partial x}+\frac{\partial M_{xy}}{\partial y}-Q_x=m_x,$$
$$\frac{\partial M_y}{\partial y}+\frac{\partial M_{xy}}{\partial x}-Q_y=m_y, \tag{3}$$
$$\frac{\partial Q_x}{\partial x}+\frac{\partial Q_y}{\partial y}=-q.$$

Substituting equation (1) into equation (3), we get the following:

$$\frac{D}{S}\left[\frac{\partial^2\psi_x}{\partial x^2}+\frac{1}{2}(1-\nu)\frac{\partial^2\psi_x}{\partial y^2}+\frac{1}{2}(1+\nu)\frac{\partial^2\psi_y}{\partial x\,\partial y}\right]-\left(\frac{\partial w}{\partial x}+\psi_x\right)=0,$$
$$\frac{D}{S}\left[\frac{\partial^2\psi_y}{\partial y^2}+\frac{1}{2}(1-\nu)\frac{\partial^2\psi_y}{\partial x^2}+\frac{1}{2}(1+\nu)\frac{\partial^2\psi_x}{\partial x\,\partial y}\right]-\left(\frac{\partial w}{\partial y}+\psi_y\right)=0,$$
$$\Delta w+\frac{\partial\psi_x}{\partial x}+\frac{\partial\psi_y}{\partial y}=0, \tag{4}$$

where $\Delta=(\partial^2/\partial x^2)+(\partial^2/\partial y^2)$ is the Laplace differential operator.

Assume that the total deflection consists of two parts which are bending deflection and transverse shear, while angles of the plate cross-sectional slope are a result of rotation of pure bending and shear angles:

$$w=w_{\mathrm{b}}+w_{\mathrm{s}},$$
$$\psi_x=\varphi_x+\theta_x, \tag{5}$$
$$\psi_y=\varphi_y+\theta_y,$$

where $\varphi_x=-(\partial w_{\mathrm{b}}/\partial x)$ and $\varphi_y=-(\partial w_{\mathrm{b}}/\partial y)$ are rotations due to pure bending and $\theta_x$ and $\theta_y$ are the shear angles.

Substituting equation (5) into equation (4), we get two differential equations:

$$\frac{\partial}{\partial x}\left(\frac{D}{S}\Delta w_{\mathrm{b}}+w_{\mathrm{s}}\right)=\frac{D}{S}\left[\frac{\partial^2\theta_x}{\partial x^2}+\frac{1}{2}(1-\nu)\frac{\partial^2\theta_x}{\partial y^2}+\frac{1}{2}(1+\nu)\frac{\partial^2\theta_y}{\partial x\,\partial y}\right]-\theta_x, \tag{6}$$

$$\frac{\partial}{\partial y}\left(\frac{D}{S}\Delta w_{\mathrm{b}}+w_{\mathrm{s}}\right)=\frac{D}{S}\left[\frac{\partial^2\theta_y}{\partial y^2}+\frac{1}{2}(1-\nu)\frac{\partial^2\theta_y}{\partial x^2}+\frac{1}{2}(1+\nu)\frac{\partial^2\theta_x}{\partial x\,\partial y}\right]-\theta_y, \tag{7}$$

$$\Delta w_s=-\left(\frac{\partial\theta_x}{\partial x}+\frac{\partial\theta_y}{\partial y}\right). \tag{8}$$

Equations (6) and (7) can be rewritten in the following forms:

$$\frac{\partial F(w_{\mathrm{b}},w_{\mathrm{s}})}{\partial x}=g_1(\theta_x,\theta_y),$$
$$\frac{\partial F(w_{\mathrm{b}},w_{\mathrm{s}})}{\partial y}=g_2(\theta_x,\theta_y), \tag{9}$$

and their integrals per $x$ and $y$ read $F(w_{\mathrm{b}},w_{\mathrm{s}})=\int g_1(\theta_x,\theta_y)\,dx=\int g_2(\theta_x,\theta_y)\,dy$; according to the structure of $g_1$ and $g_2$ in equations (6) and (7), the reasonable solution is that both $g_1$ and $g_2$ must be set to zero; as a consequence of that consideration, the relation between transverse shear and bending is

$$w_{\mathrm{s}}=-\frac{D}{S}\Delta w_{\mathrm{b}}. \tag{10}$$

The total deflection is

$$w=w_{\mathrm{b}}-\frac{D}{S}\Delta w_{\mathrm{b}}. \tag{11}$$

Using the new modified first-order shear deformation theory, the displacement field of the plate can be rewritten in the following form [26]:

$$u(x,y,z)=u(x,y)-z\varphi_x,$$
$$v(x,y,z)=v(x,y)-z\varphi_y, \tag{12}$$
$$w(x,y,z)=w_{\mathrm{b}}(x,y)+w_{\mathrm{s}}(x,y).$$

The strain-displacement relations may be written as follows [26]:

$$\varepsilon_x=\frac{\partial u}{\partial x}-z\frac{\partial^2 w_{\mathrm{b}}}{\partial x^2},$$
$$\varepsilon_y=\frac{\partial v}{\partial y}-z\frac{\partial^2 w_{\mathrm{b}}}{\partial y^2},$$
$$\gamma_{xy}=\frac{\partial u}{\partial y}+\frac{\partial v}{\partial x}-2z\frac{\partial^2 w_{\mathrm{b}}}{\partial x\,\partial y}, \tag{13}$$
$$\gamma_{xz}=\frac{\partial w_{\mathrm{s}}}{\partial x},$$
$$\gamma_{yz}=\frac{\partial w_{\mathrm{s}}}{\partial y}.$$

Equation (13) can be rewritten in the matrix form as

$$\boldsymbol{\varepsilon}=\boldsymbol{\varepsilon}^0+z\boldsymbol{\varepsilon}^1, \tag{14}$$

where

$$\boldsymbol{\varepsilon}^0=\begin{Bmatrix}\dfrac{\partial u}{\partial x}\\[2mm]\dfrac{\partial v}{\partial y}\\[2mm]\dfrac{\partial u}{\partial y}+\dfrac{\partial v}{\partial x}\end{Bmatrix},$$
$$\boldsymbol{\varepsilon}^1=-\begin{Bmatrix}\dfrac{\partial^2 w_b}{\partial x^2}\\[2mm]\dfrac{\partial^2 w_b}{\partial y^2}\\[2mm]2\dfrac{\partial^2 w_b}{\partial x\,\partial y}\end{Bmatrix}, \tag{15}$$

and

$$\boldsymbol{\gamma} = \begin{Bmatrix} \dfrac{\partial w_s}{\partial x} \\ \dfrac{\partial w_s}{\partial y} \end{Bmatrix}. \tag{16}$$

*2.2.2. Finite Element Formulations.* The plate is discretized using the quadrilateral four-node element, as shown in Figure 2. Each node has nine degrees of freedom including four axial, one transversal, and four rotational displacements.

The element nodal displacement vector can be given as

$$\mathbf{q} = \{\mathbf{q}_1 \;\; \mathbf{q}_2 \;\; \mathbf{q}_3 \;\; \mathbf{q}_4\}^T, \tag{17}$$

where

$$\mathbf{q}_j = \{u_j^m \;\; v_j^m \;\; u_j^n \;\; v_j^n \;\; w_j \;\; \varphi_{xj}^m \;\; \varphi_{yj}^m \;\; \varphi_{xj}^n \;\; \varphi_{yj}^n\}^T, \quad j = \overline{1,4}. \tag{18}$$

The nodal displacement vector of each component is

$$\mathbf{q}_i = \{\mathbf{q}_{1i} \;\; \mathbf{q}_{2i} \;\; \mathbf{q}_{3i} \;\; \mathbf{q}_{4i}\}^T, \quad i = m, n, \tag{19}$$

where

$$\mathbf{q}_{ji} = \{u_j^i \;\; v_j^i \;\; w_j \;\; \varphi_{xj}^i \;\; \varphi_{yj}^i\}^T, \quad j = \overline{1,4}, \; i = m, n. \tag{20}$$

In equations (18) and (20), $u$, $v$, and $w$ are, respectively, the $x-$ and $y$-axis displacements and transversal displacement and $\varphi_x$ and $\varphi_y$ denote the bending rotations of the $x-$ and $y-$axis, respectively.

The static bending deflection $w_b$ is assumed in a polynomial form. Then, the transverse shear $w_s$ and bending rotations $\varphi_x$ and $\varphi_y$ are calculated using the above equations, while the axial displacements $u$ and $v$ are approximated using Lagrangian shape functions.

The displacements $u$ and $v$ may be approximated as

$$u = \sum_{j=1}^{4} N_j u_j, \qquad v = \sum_{j=1}^{4} N_j v_j, \tag{21}$$

where

$$N_j = \frac{1}{4}\left(1 - \xi_j \xi\right)\left(1 - \eta_j \eta\right), \quad j = \overline{1,4}. \tag{22}$$

The bending deflection $w_b$ is approximated using a polynomial form as

$$w_{bi} = \mathbf{P}_{bi}\mathbf{a}_i, \quad i = m, n, \tag{23}$$

where $\mathbf{a}_i$ is a vector of polynomial coefficients and

$$\mathbf{P}_{bi} = \left[1, \xi, \eta, \xi^2, \xi\eta, \eta^2, \xi^3, \xi^2\eta, \xi\eta^2, \eta^3, \xi^3\eta, \xi\eta^3\right], \quad i = m, n, \tag{24}$$

where $\xi = (2x - a)/a, \eta = (2y - b)/b$. According to equation (10), the transverse shear is given by

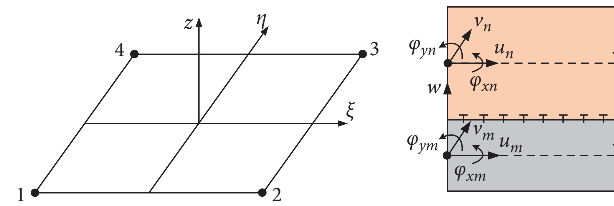


(a) (b)

Figure 2: A two-layer composite plate element.

$$w_{si} = -\frac{D_i}{S_i}\Delta w_{bi} = \mathbf{P}_{si}\mathbf{a}_i, \tag{25}$$

where

$$\mathbf{P}_{si} = -[0, 0, 0, 2\alpha_i, 0, 2\beta_i, 6\alpha_i\xi, 2\alpha_i\eta, 2\beta_i\xi, 6\beta_i\eta, 6\alpha_i\xi\eta, 6\beta_i\xi\eta], \quad i = m, n, \tag{26}$$

in which $\alpha_i = (4D_i/S_i a^2)$, $\beta = (4D_i/S_i b^2)$.

The total static deflection of the plate is

$$w_i = w_{bi} + w_{si} = (\mathbf{P}_{bi} + \mathbf{P}_{si})\mathbf{a}_i, \quad i = m, n. \tag{27}$$

The rotations of cross sections on the neutral plane are

$$\begin{aligned} \varphi_{xi} &= -\frac{2}{a}\frac{\partial \mathbf{P}_{bi}}{\partial \xi}\mathbf{a}_i \\ &= -\frac{2}{a}\left[0, 1, 0, 2\xi, \eta, 0, 3\xi^2, 2\xi\eta, \eta^2, 0, 3\xi^2\eta, \eta^3\right]\mathbf{a}_i \\ &= \mathbf{P}_{\varphi xi}\mathbf{a}_i, \quad i = m, n, \end{aligned} \tag{28}$$

$$\begin{aligned} \varphi_{yi} &= -\frac{2}{b}\frac{\partial \mathbf{P}_{bi}}{\partial \eta}\mathbf{a}_i \\ &= -\frac{2}{b}\left[0, 0, 1, 0, \xi, 2\eta, 0, \xi^2, 2\xi\eta, 3\eta^2, \xi^3, 3\xi\eta^2\right]\mathbf{a}_i \\ &= \mathbf{P}_{\varphi yi}\mathbf{a}_i, \quad i = m, n. \end{aligned} \tag{29}$$

Taking coordinate values $\xi$ and $\eta$ for each node into equations (27)–(29), we get

$$\mathbf{d}_i = \mathbf{C}_i\mathbf{a}_i \Longrightarrow \mathbf{a}_i = \mathbf{C}_i - 1\mathbf{d}_i, \quad i = m, n, \tag{30}$$

where $\mathbf{d}_i = \{\mathbf{d}_{1i} \;\; \mathbf{d}_{2i} \;\; \mathbf{d}_{3i} \;\; \mathbf{d}_{4i}\}^T$ ($\mathbf{d}_{ji} = \{w_{ji} \;\; \varphi_{xji} \;\; \varphi_{yji}\}^T$, $j = \overline{1,4}$, $i = m, n$), and matrix $\mathbf{C}_i$ is shown in Appendix.

Taking equation (30) into account, we get

$$w_{bi} = \mathbf{P}_{bi}\mathbf{C}_i - 1\mathbf{d}_i = \mathbf{Q}_{bi}\mathbf{d}_i, \quad i = m, n, \tag{31}$$

$$w_{si} = \mathbf{P}_{si}\mathbf{C}_i^{-1}\mathbf{d}_i = \mathbf{Q}_{si}\mathbf{d}_i, \quad i = m, n, \tag{32}$$

$$w_i = w_{bi} + w_{si} = (\mathbf{P}_{bi} + \mathbf{P}_{si})\mathbf{C}_i^{-1}\mathbf{d}_i = \mathbf{P}_i\mathbf{C}_i^{-1}\mathbf{d}_i, \quad i = m, n. \tag{33}$$

Substituting equations (21) and (31) into equation (14), we obtain

$$\boldsymbol{\varepsilon}_i = \mathbf{L}_{0i}\mathbf{u}_i + z_i\mathbf{L}_{1i}\mathbf{d}_i = [\mathbf{L}_{0i} \;\; z_i\mathbf{L}_{1i}]\begin{Bmatrix}\mathbf{u}_i \\ \mathbf{d}_i\end{Bmatrix} = [\mathbf{L}_{0i} \;\; z_i\mathbf{L}_{1i}]\mathbf{q}_i, \tag{34}$$

where

$$\mathbf{L}_{0i} = \left[\, \mathbf{L}_{01i} \;\; \mathbf{L}_{02i} \;\; \mathbf{L}_{03i} \;\; \mathbf{L}_{04i} \,\right],\; \mathbf{L}_{0ji} = \begin{bmatrix} \dfrac{\partial N_j}{\partial x} & 0 \\ 0 & \dfrac{\partial N_j}{\partial y} \\ \dfrac{\partial N_j}{\partial y} & \dfrac{\partial N_j}{\partial x} \end{bmatrix}, \quad j = \overline{1,4},\; i = m, n. \tag{35}$$

$$\mathbf{L}_{1i} = \mathbf{H}_{bi}\mathbf{C}_i^{-1},\; \mathbf{H}_{bi} = \begin{bmatrix} \dfrac{4}{a^2}\dfrac{\partial^2 \mathbf{P}_{bi}}{\partial \xi^2} \\ \dfrac{4}{b^2}\dfrac{\partial^2 \mathbf{P}_{bi}}{\partial \eta^2} \\ \dfrac{4}{ab}\dfrac{\partial^2 \mathbf{P}_{bi}}{\partial \xi\,\partial \eta} \end{bmatrix}, \quad i = m, n. \tag{36}$$

By substituting equation (25) into equation (16), we get

$$\boldsymbol{\gamma}_i = \mathbf{L}_{si}\mathbf{d}_i, \quad i = m, n, \tag{37}$$

where

$$\mathbf{L}_{si} = \mathbf{H}_{si}\mathbf{C}_i^{-1},\; \mathbf{H}_{si} = \begin{bmatrix} \dfrac{2}{a}\dfrac{\partial \mathbf{P}_{si}}{\partial \xi} \\ \dfrac{2}{b}\dfrac{\partial \mathbf{P}_{si}}{\partial \eta} \end{bmatrix}, \quad i = m, n. \tag{38}$$

According to Hooke's law, the relationship between stresses and strains can be given as

$$\boldsymbol{\sigma}_i = \mathbf{D}_i\boldsymbol{\varepsilon}_i,\; \boldsymbol{\tau}_i = \mathbf{G}_i\boldsymbol{\gamma}_i, \quad i = m, n, \tag{39}$$

where

$$\mathbf{D}_i = \frac{E_i}{1-\nu_i^2}\begin{bmatrix} 1 & \nu_i & 0 \\ \nu_i & 1 & 0 \\ 0 & 0 & \dfrac{(1-\nu_i)}{2} \end{bmatrix},$$
$$\mathbf{G}_i = \frac{kE_i}{2(1+\nu_i)}\begin{bmatrix} 1 & 0 \\ 0 & 1 \end{bmatrix}, \quad i = m, n. \tag{40}$$

The calculation model for the connector stub is shown in Figure 3.

By using Lagrangian approximation for both axial displacement and rotation of two components to determine the axial deflection of the connector stub, the interfacial slips of two components are given by

$$\boldsymbol{\delta}_{st} = \begin{Bmatrix} u_{st} \\ v_{st} \end{Bmatrix} = \begin{Bmatrix} u_n\left(\dfrac{-h_n}{2}\right) \\ v_n\left(\dfrac{-h_n}{2}\right) \end{Bmatrix} - \begin{Bmatrix} u_m\left(\dfrac{-h_n}{2}\right) \\ v_m\left(\dfrac{-h_n}{2}\right) \end{Bmatrix}$$
$$= \begin{bmatrix} u_{n0} - u_{m0} + \dfrac{(h_n\varphi_{xn} - h_m\varphi_{xm})}{2} \\ v_{n0} - v_{m0} + \dfrac{(h_n\varphi_{yn} - h_m\varphi_{ym})}{2} \end{bmatrix} = \mathbf{N}_{st}\mathbf{q}_e, \tag{41}$$

where

$$\mathbf{N}_{st} = \left[\, \mathbf{N}_{st}^1 \;\; \mathbf{N}_{st}^2 \;\; \mathbf{N}_{st}^3 \;\; \mathbf{N}_{st}^4 \,\right], \tag{42}$$

$$\mathbf{N}_{st}^j = \begin{bmatrix} -N_j & 0 & N_j & 0 & 0 & -0.5h_mN_j & 0 & 0.5h_nN_j & 0 \\ 0 & -N_j & 0 & N_j & 0 & 0 & -0.5h_mN_j & 0 & 0.5h_nN_j \end{bmatrix}, \quad j = \overline{1,4}, \tag{43}$$

in which $u_{st}$ and $v_{st}$ are the deflections of the connector stub.

The strain energy of two components and connector stub can be given by

$$\prod_e = \prod_e^{p} + \prod_e^{st} = \sum_{i=m,n}\frac{1}{2}\int_{A_e}\int_{h_i}\left(\boldsymbol{\varepsilon}_i^T\mathbf{D}_i\boldsymbol{\varepsilon}_i + \boldsymbol{\tau}_i^T\mathbf{G}_i\boldsymbol{\gamma}_i\right)dz_i dA + \frac{1}{2}\int_{A_e}k_{st}\left(u_{st}^2 + v_{st}^2\right)dA$$
$$= \sum_{i=m,n}\frac{1}{2}\int_{A_e}\int_{h_i}\left(\boldsymbol{\varepsilon}_i^T\mathbf{D}_i\boldsymbol{\varepsilon}_i + \boldsymbol{\tau}_i^T\mathbf{G}_i\boldsymbol{\gamma}_i\right)\, dz_i dA + \frac{1}{2}\int_{A_e}\mathbf{q}_e^T\mathbf{N}_{st}^T k_{st}\mathbf{N}_{st}\mathbf{q}_e dA. \tag{44}$$

The kinetic energy is

$$T_e = \frac{1}{2}\sum_{i=m,n}\int_{A_e}\int_{h_i}\rho_i\dot{w}^2\, dz_i dA, \tag{45}$$

or

$$T_e = \frac{1}{2}\sum_{i=m,n}\int_{A_e}\int_{h_i}\dot{d}_i^T\mathbf{C}_i^{-T}\mathbf{P}_i^T\rho_i\mathbf{P}_i\mathbf{C}_i^{-T}\dot{d}_i\, dz_i dA. \tag{46}$$

Equation (46) can be rewritten in the shorter form as follows:

$$T_e = \frac{1}{2}\sum_{i=m,n}\int_{A_e}\widehat{m}_i\dot{d}_i^T\mathbf{C}_i^{-T}\mathbf{P}_i^T\mathbf{P}_i\mathbf{C}_i^{-T}\dot{d}_i dA, \tag{47}$$

where $\widehat{m}_i = \int_{h_i}\rho_i dz_i,\; i = m, n.$

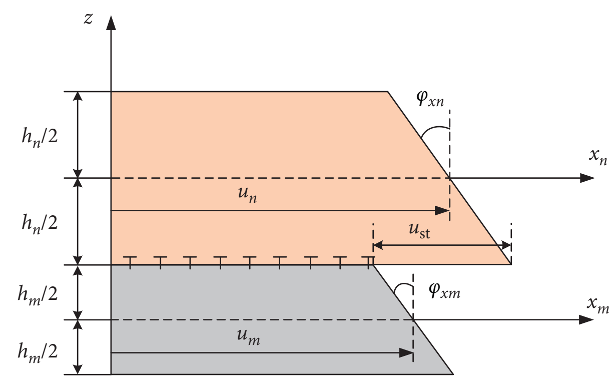


FIGURE 3: Axial displacement assuming a two-layer composite plate with connector stubs.

The work done by external distribution normal force acting on the top surface of layer $n$ is

$$V_e = \int_{A_e} qw \, dA = \int_{A_e} q\mathbf{Q}_n\mathbf{d}_n dA, \tag{48}$$

where $q$ is the uniform load.

The Lagrangian function of the plate element is defined by

$$L_e = T_e - \prod_e. \tag{49}$$

Using Lagrange's equations, the governing equations of motion of the plate element are given by

$$\frac{d}{dt}\left(\frac{\partial L_e}{\partial \dot{q}_e}\right) - \frac{\partial L_e}{\partial \mathbf{q}_e} = \frac{\partial V_e}{\partial \mathbf{q}_e}. \tag{50}$$

Substituting equations (44), (46), and (48) into equation (50) considering equation (49), the equation of motion of the plate can be obtained in the matrix form as

$$\left(\mathbf{M}_e^m + \mathbf{M}_e^n\right)\ddot{q}_e + \left(\mathbf{K}_e^m + \mathbf{K}_e^n + \mathbf{K}_e^{st}\right)\mathbf{q}_e = \left(\mathbf{F}_e^m + \mathbf{F}_e^n\right), \tag{51}$$

in which $\mathbf{M}_e^i$, $\mathbf{K}_e^i$ and $\mathbf{K}_e^{st}$, and $\mathbf{F}_e^i$ are, respectively, the element mass matrix, the element stiffness matrix, and element force vector, which are defined as

$$\mathbf{M}_e^i = \frac{ab}{4}\widehat{m}_i \int_{-1}^{1}\int_{-1}^{1} \mathbf{C}_i^{-T}\mathbf{P}_i^T\mathbf{P}_i\mathbf{C}_i^{-T} d\xi \, d\eta, \quad i = m, n, \tag{52}$$

$$\mathbf{K}_e^i = \frac{ab}{4}\int_{-1}^{1}\int_{-1}^{1}\int_{h_i} \left[\mathbf{L}_{0i} \;\; z_i\mathbf{L}_{1i}\right]^T \mathbf{D}_i \left[\mathbf{L}_{0i} \;\; z_i\mathbf{L}_{1i}\right] dz_i d\xi \, d\eta + \frac{ab}{4}\int_{-1}^{1}\int_{-1}^{1}\int_{h_i} \mathbf{L}_{si}^T\mathbf{G}_i\mathbf{L}_{si} dz_i d\xi \, d\eta, \quad i = m, n, \tag{53}$$

$$\mathbf{K}_e^{st} = \frac{ab}{4}\int_{-1}^{1}\int_{-1}^{1} \mathbf{N}_{st}^T k_{st}\mathbf{N}_{st} d\xi \, d\eta, \tag{54}$$

$$\mathbf{F}_e^n = \frac{ab}{4}\int_{-1}^{1}\int_{-1}^{1} q\mathbf{Q}_n d\xi \, d\eta, \quad \mathbf{F}_e^m = 0. \tag{55}$$

Note that we need not any selective reduced integration or reduced integration scheme to calculate the matrices and vectors in equations (52)–(55). When $k_{st}$ gets a high value, displacements of the top and bottom layers at the contact surface are the same; from equation (41), the stiffness matrix of the stub in equation (54) gets the value 0: it means that the structure has no stubs and then the displacement is continuous at the interfaces between two layers. After assembling the element matrix and the element vector into the global matrix and global vector, the governing equation of motion of the plate is obtained as

$$\mathbf{M}\ddot{U} + \mathbf{KU} = \mathbf{F}, \tag{56}$$

where $\mathbf{M}$, $\mathbf{K}$, and $\mathbf{F}$ are, respectively, the global mass matrix, global stiffness matrix, and global force vector and $\mathbf{U}$ is the vector of unknown nodal displacements.

*2.3. Static Bending and Free Vibration Problem.* For the static bending problem, ignoring $\ddot{U}$, equation (56) becomes

$$\mathbf{KU} = \mathbf{F}. \tag{57}$$

Solving equation (57), we get the vector of unknown nodal displacements $\mathbf{U}$.

For free vibration analysis, neglecting the effect of external force vector $\mathbf{F}$ and assuming $\mathbf{u} = \mathbf{U}e^{i\omega t}$ in equation (56), we get the following eigenvalue problem:

$$\left(\mathbf{K} - \omega^2\mathbf{M}\right)\mathbf{U} = 0. \tag{58}$$

Solving equation (58), we get $\omega$, which denotes the natural frequencies of the plate; for each value of $\omega$, we have an eigenvector.

## 3. Numerical Results and Discussion

We now focus on numerically studying the static bending and free vibration responses of the two-layer composite plate. Each edge of the plate can be under the simply supported boundary condition or clamped boundary condition. For the simply supported edge,

$$v_n = v_m = w = 0, \;\; \varphi_{yn} = \varphi_{ym} = 0, \quad \text{at } x = 0, a, \tag{59a}$$

$$u_n = u_m = w = 0, \;\; \varphi_{xn} = \varphi_{xm} = 0, \quad \text{at } y = 0, b. \tag{59b}$$

For the clamped edge,

$$u_n = u_m = v_n = v_m = w = 0, \quad \varphi_{xn} = \varphi_{xm} = \varphi_{yn} = \varphi_{ym} = 0, \quad \text{at } x = 0, \; a \text{ and } y = 0, \; b. \tag{60}$$

*3.1. Static Bending Analysis of Two-Layer Composite Plates*

*3.1.1. Accuracy Studies.* To verify the proposed method, we compare the deflections in two cases of materials: homogeneous and composite materials. Firstly, a square homogeneous plate under contribution load $q = -1N$ is investigated, and the length and the width are $a = b = 1$ m. The plate is simply supported at all edges (SSSS) or fully clamped (CCCC). In the published works [27, 28], the plate has one layer made of homogeneous material with $E = 10920$ MPa, Poisson's ratio $\nu = 0.3$, and the thickness $h$. But in this work, we assume that the plate has two layers connected by stubs with two cases—case 1: $h_n = 0.999\,h$, $h_m = 0.001\,h$, and $k_{st} = 0$ and case 2: $h_n = h_m = 0.5\,h$ and $k_{st} = 10^{10}E$. In both cases, material properties of two layers are set to be $E_n = E_m = E = 10920$ MPa and $\nu_n = \nu_m = \nu = 0.3$, thicknesses of the top and bottom layer are $h_n$ and $h_m$, respectively, and $h_n + h_m = h$. The nondimensional deflection is defined as

$$\overline{w} = w_{\max}\frac{D}{qa^4}, \tag{61}$$

where $D$ is given in equation (2).

Table 1 shows a comparison of the nondimensional deflections of SSSS and CCCC plates obtained by this method and other approaches (FEM [28] and analytical solution [28]). We meet a good agreement among three solutions.

We see that when the thickness of one layer is much higher than that of the other layer and the stiffness of the connector stub is very small, the behavior of the two-layer plate is the same as the behavior of the one-layer plate with the same thickness. In addition, when two layers have the same thickness and material, the stiffness of the connector stub gets a much higher value $k_{st} = 10_{10}E$, and then the two-layer plate is considered as the one-layer plate with the thickness equal to the sum of thickness of the two components.

In order to further confirm the accuracy of this method, we compare the nondimensional deflection of a square SSSS composite plate ($a/b = 1$ and the total thickness $h = a/10$) with two layers ($0/90^\circ$) which have the same thickness $h/2$; the material properties are $E_1/E_2 = 25$, $G_{12} = G_{13} = 0.5E_2$, $G_{23} = 0.2E_2$, and $\nu_{12} = 0.25$. In this comparison, the plate is modeled as $h_n = h_m = 0.5\,h$, $k_{st} = 10^{10}E_2$, and the fiber directions of the top and bottom layers are $0^\circ$ and $90^\circ$, respectively. Table 2 shows the comparison of the nondimensional deflection of this composite plate subjected to uniformly distributed load and central concentrated load. The nondimensional deflection of the plate is calculated by the following formula:

$$\overline{w} = w_{\max}\frac{100E_2h^3}{a^4q}. \tag{62}$$

It is shown plainly that the present results have a good agreement with the results given in [29] (analytical method). According to the above two comparisons, the present results have a good agreement with other published ones.

*3.1.2. Numerical Results for Static Bending Analysis of Two-Layer Composite Plates.* In this section, a rectangular two-layer composite plate subjected to the uniform load $q$ is investigated. The boundary conditions of the plate are SSSS (fully simply supported), CCCC (fully clamped), CSCS (two opposite edges are simply supported and two other edges are clamped), and CCSS (two adjacent edges are clamped and two other edges are simply supported). The sides, thickness, and material properties of the plate are set to be $a = 1$ m, $h = a/100$, $E_m = 200$ GPa, $E_n = 10$ GPa, $a/b$ = open, $h_n/h_m$ = open, and $k_{st}/E_m$ = open. The nondimensional displacement of this plate is normalized by

$$\overline{w} = w\frac{100E_mh^3}{12qa^4\left(1-\nu_m^2\right)}. \tag{63}$$

*(1) Influence of the Length-to-Width Ratio a/b.* In order for studying the effect of the aspect ratio $a/b$ on the mechanical bending behavior of the two-layer composite plate, this ratio is set to vary from 0.5 to 4, while $h_n/h_m = 1$, $h_n/h_m = 2$, and the ratio of stiffness of the connector stub $k_{st}/E_m = 1$ are considered. The computed results are shown in Table 3 and Figures 4(a) and 4(b). According to Table 3 and Figure 4, it is seen that when the aspect ratio $a/b$ increases, the nondimensional deflection decreases. In addition, when the ratio $(a/b) > 3$, the nondimensional deflections of both boundary conditions CCCC and CSCS of plates are very close to each other.

*(2) Influence of the Thickness-to-Thickness Ratio $h_n/h_m$.* Next, the research on the variation of deflection affected by the relationship between the bottom layer thickness and the top layer thickness is now investigated. The ratio $h_n/h_m$ increases from 1 to 4, $k_{st}/E_m = 1$, and the length-to-width ratio $a/b$ is set to be 1 and 2. The nondimensional deflection of the plate with different boundary conditions is shown in Table 4 and Figure 5. The deflection of the plate increases when increasing ratio $h_n/h_m$; this can be explained by the fact that Young's modulus of the layer $n$ is less than that of layer $m$, and the stiffness of the two-layer plate becomes smaller when the ratio $h_n/h_m$ increases.

*(3) Influence of the Stiffness of the Connector Stub.* Table 5 and Figure 6 show the nondimensional deflections as a function of the ratio $k_{st}/E_m$ of a square two-layer composite plate with $h_n/h_m = 1$ and $h_n/h_m = 2$. The stiffness of the stub varies from 0 to $10^6E_m$; when it changes from 0 to $E_m$, this plate is stiffer and the deflection decreases; but when the stiffness of the stub $> E_m$, then the effect of the stub goes to zero so that the two-layer plate connected by the stub becomes a two-layer one with no stub and the displacements at the contact place are the same; it means that there is no slip between two layers at the contact place.

To show clearly the slip between the top and bottom layers at the contact place, we depicted the ratio $R_{mn}^1$ and $R_{mn}^2$ in Figures 7 and 8, respectively, in which $R_{mn}^1$ and $R_{mn}^2$ are defined as

$$R_{mn}^1 = \left|u_m\left(\frac{a}{4},\frac{b}{2},\frac{h_m}{2}\right) - u_n\left(\frac{a}{4},\frac{b}{2},\frac{-h_n}{2}\right)\right|\frac{1000E_mh^3}{12qa^4\left(1-\nu_m^2\right)},$$
$$R_{mn}^2 = \left|u_m\left(x,\frac{b}{2},\frac{h_m}{2}\right) - u_n\left(x,\frac{b}{2},\frac{-h_n}{2}\right)\right|\frac{1000E_mh^3}{12qa^4\left(1-\nu_m^2\right)}. \tag{64}$$

Table 1: Comparison of nondimensional deflection of square plates with $a/h = 10$ and $a/h = 10000$.

| Source | SSSS | | CCCC | |
|---|---|---|---|---|
| | $a/h = 10$ | $a/h = 10000$ | $a/h = 10$ | $a/h = 10000$ |
| Ferreira [28] | 0.004271 | 0.004060 | 0.001503 | 0.001264 |
| Exact solution [28] | 0.004270 | 0.004060 | — | 0.001260 |
| Present ($h_n = 0.999\,h$, $h_m = 0.001\,h$, and $k_{st} = 0$) | 0.004290 | 0.004079 | 0.001508 | 0.001272 |
| Present ($h_n = h_m = 0.5\,h$ and $k_{st} = 10^{10}E$) | 0.004300 | 0.004079 | 0.001523 | 0.001291 |

Table 2: Comparison of the nondimensional deflection of a square SSSS composite plate subject to uniformly distributed load and central concentrated load.

| $\overline{w}$ | Uniformly distributed load | | Central concentrated load | |
|---|---|---|---|---|
| | Reddy [29] | Present | Reddy [29] | Present |
| | 1.6955 | 1.6538 | 4.6664 | 4.6421 |

Table 3: Nondimensional deflection of the plate as a function of ratio $a/b$ with $k_{st}/E_m = 1$.

| $a/b$ | $h_n/h_m = 1$ | | | | $h_n/h_m = 2$ | | | |
|---|---|---|---|---|---|---|---|---|
| | SSSS | CCCC | CSCS | CCSS | SSSS | CCCC | CSCS | CCSS |
| 0.5 | 6.4728 | 1.6252 | 5.4088 | 3.1243 | 12.5027 | 3.1584 | 10.4767 | 6.0528 |
| 0.625 | 5.3098 | 1.4770 | 3.8595 | 2.7089 | 10.2589 | 2.8726 | 7.4844 | 5.2510 |
| 0.75 | 4.2368 | 1.2639 | 2.6511 | 2.2449 | 8.1874 | 2.4598 | 5.1458 | 4.3531 |
| 0.875 | 3.3289 | 1.0313 | 1.8013 | 1.7999 | 6.4339 | 2.0083 | 3.4991 | 3.4914 |
| 1.0 | 2.5968 | 0.8135 | 1.2304 | 1.4124 | 5.0196 | 1.5849 | 2.3919 | 2.7406 |
| 1.2 | 1.7421 | 0.5350 | 0.6889 | 0.9375 | 3.3683 | 1.0431 | 1.3408 | 1.8201 |
| 1.4 | 1.1793 | 0.3464 | 0.4036 | 0.6196 | 2.2806 | 0.6760 | 0.7866 | 1.2035 |
| 1.6 | 0.8107 | 0.2259 | 0.2475 | 0.4139 | 1.5683 | 0.4413 | 0.4830 | 0.8046 |
| 1.8 | 0.5676 | 0.1501 | 0.1582 | 0.2818 | 1.0984 | 0.2936 | 0.3094 | 0.5482 |
| 2.0 | 0.4050 | 0.1020 | 0.1051 | 0.1958 | 0.7839 | 0.1999 | 0.2058 | 0.3812 |
| 2.2 | 0.2943 | 0.0711 | 0.0721 | 0.1389 | 0.5699 | 0.1395 | 0.1416 | 0.2707 |
| 2.4 | 0.2177 | 0.0507 | 0.0510 | 0.1006 | 0.4217 | 0.0997 | 0.1003 | 0.1962 |
| 2.6 | 0.1637 | 0.0370 | 0.0371 | 0.0742 | 0.3172 | 0.0729 | 0.0730 | 0.1450 |
| 2.8 | 0.1249 | 0.0276 | 0.0275 | 0.0558 | 0.2423 | 0.0544 | 0.0544 | 0.1091 |
| 3.0 | 0.0967 | 0.0209 | 0.0209 | 0.0426 | 0.1877 | 0.0415 | 0.0414 | 0.0835 |
| 3.2 | 0.0759 | 0.0162 | 0.0162 | 0.0331 | 0.1473 | 0.0321 | 0.0322 | 0.0650 |
| 3.4 | 0.0602 | 0.0127 | 0.0127 | 0.0261 | 0.1170 | 0.0253 | 0.0254 | 0.0512 |
| 3.6 | 0.0484 | 0.0101 | 0.0101 | 0.0208 | 0.0940 | 0.0202 | 0.0203 | 0.0409 |
| 3.8 | 0.0392 | 0.0082 | 0.0082 | 0.0168 | 0.0763 | 0.0164 | 0.0164 | 0.0331 |
| 4.0 | 0.0321 | 0.0067 | 0.0067 | 0.0137 | 0.0626 | 0.0134 | 0.0134 | 0.0270 |

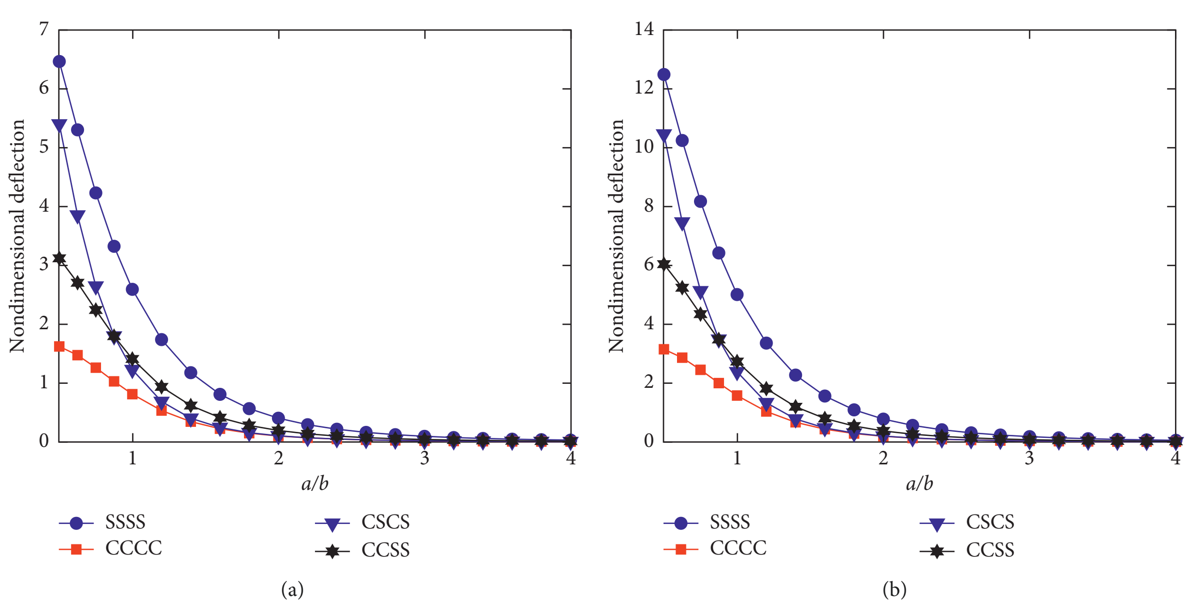


Figure 4: The influence of ratio $a/b$ on the nondimensional deflection of the plate with $k_{st}/E_m = 1$: (a) $h_n/h_m = 1$; (b) $h_n/h_m = 2$.

Table 4: Nondimensional deflection of the plate as a function of ratio $h_n/h_m$ with $k_{st}/E_b = 1$.

| $h_n/h_m$ | $a/b = 1$ | | | | $a/b = 2$ | | | |
|---|---|---|---|---|---|---|---|---|
| | SSSS | CCCC | CSCS | CCSS | SSSS | CCCC | CSCS | CCSS |
| 1.0 | 2.5968 | 0.8135 | 1.2304 | 1.4124 | 0.4050 | 0.1020 | 0.1051 | 0.1958 |
| 1.2 | 3.1576 | 0.9907 | 1.4977 | 1.7187 | 0.4926 | 0.1243 | 0.1281 | 0.2384 |
| 1.4 | 3.6969 | 1.1617 | 1.7556 | 2.0138 | 0.5769 | 0.1460 | 0.1503 | 0.2795 |
| 1.6 | 4.1941 | 1.3201 | 1.9940 | 2.2864 | 0.6546 | 0.1661 | 0.1710 | 0.3175 |
| 1.8 | 4.6367 | 1.4618 | 2.2070 | 2.5297 | 0.7239 | 0.1841 | 0.1896 | 0.3516 |
| 2.0 | 5.0196 | 1.5849 | 2.3919 | 2.7406 | 0.7839 | 0.1999 | 0.2058 | 0.3812 |
| 2.2 | 5.3436 | 1.6895 | 2.5488 | 2.9194 | 0.8348 | 0.2133 | 0.2196 | 0.4063 |
| 2.4 | 5.6129 | 1.7769 | 2.6798 | 3.0684 | 0.8771 | 0.2246 | 0.2312 | 0.4273 |
| 2.6 | 5.8338 | 1.8489 | 2.7875 | 3.1909 | 0.9118 | 0.2340 | 0.2408 | 0.4447 |
| 2.8 | 6.0131 | 1.9077 | 2.8752 | 3.2906 | 0.9400 | 0.2416 | 0.2487 | 0.4588 |
| 3.0 | 6.1575 | 1.9552 | 2.9461 | 3.3710 | 0.9628 | 0.2478 | 0.2551 | 0.4702 |
| 3.2 | 6.2731 | 1.9934 | 3.0030 | 3.4355 | 0.9810 | 0.2529 | 0.2603 | 0.4795 |
| 3.4 | 6.3651 | 2.0239 | 3.0485 | 3.4870 | 0.9956 | 0.2569 | 0.2644 | 0.4868 |
| 3.6 | 6.4379 | 2.0482 | 3.0847 | 3.5278 | 1.0071 | 0.2602 | 0.2678 | 0.4927 |
| 3.8 | 6.4954 | 2.0676 | 3.1133 | 3.5602 | 1.0162 | 0.2628 | 0.2704 | 0.4974 |
| 4.0 | 6.5405 | 2.0828 | 3.1359 | 3.5856 | 1.0234 | 0.2649 | 0.2726 | 0.5011 |

Table 5: Nondimensional deflection of the plate as a function of ratio $k_{st}/E_m$ with $a/b = 1$.

| $k_{st}/E_m$ | $h_n/h_m = 1$ | | | | $h_n/h_m = 2$ | | | |
|---|---|---|---|---|---|---|---|---|
| | SSSS | CCCC | CSCS | CCSS | SSSS | CCCC | CSCS | CCSS |
| 0 | 3.1903 | 0.9951 | 1.5068 | 1.7316 | 9.4673 | 2.9526 | 4.4712 | 5.1381 |
| $10^{-2}$ | 2.6790 | 0.8708 | 1.3056 | 1.4862 | 5.5538 | 1.9698 | 2.8925 | 3.2279 |
| $10^{-1}$ | 2.6051 | 0.8214 | 1.2402 | 1.4215 | 5.0730 | 1.6363 | 2.4560 | 2.7995 |
| $10^{0}$ | 2.5968 | 0.8135 | 1.2304 | 1.4124 | 5.0196 | 1.5849 | 2.3919 | 2.7406 |
| $10^{1}$ | 2.5959 | 0.8126 | 1.2293 | 1.4114 | 5.0142 | 1.5792 | 2.3850 | 2.7343 |
| $10^{2}$ | 2.5958 | 0.8125 | 1.2292 | 1.4113 | 5.0137 | 1.5787 | 2.3843 | 2.7336 |
| $10^{3}$ | 2.5958 | 0.8125 | 1.2292 | 1.4113 | 5.0136 | 1.5786 | 2.3842 | 2.7336 |
| $10^{4}$ | 2.5958 | 0.8125 | 1.2292 | 1.4113 | 5.0136 | 1.5786 | 2.3842 | 2.7336 |
| $10^{5}$ | 2.5958 | 0.8125 | 1.2292 | 1.4113 | 5.0136 | 1.5786 | 2.3842 | 2.7336 |
| $10^{6}$ | 2.5958 | 0.8125 | 1.2292 | 1.4113 | 5.0136 | 1.5786 | 2.3842 | 2.7336 |

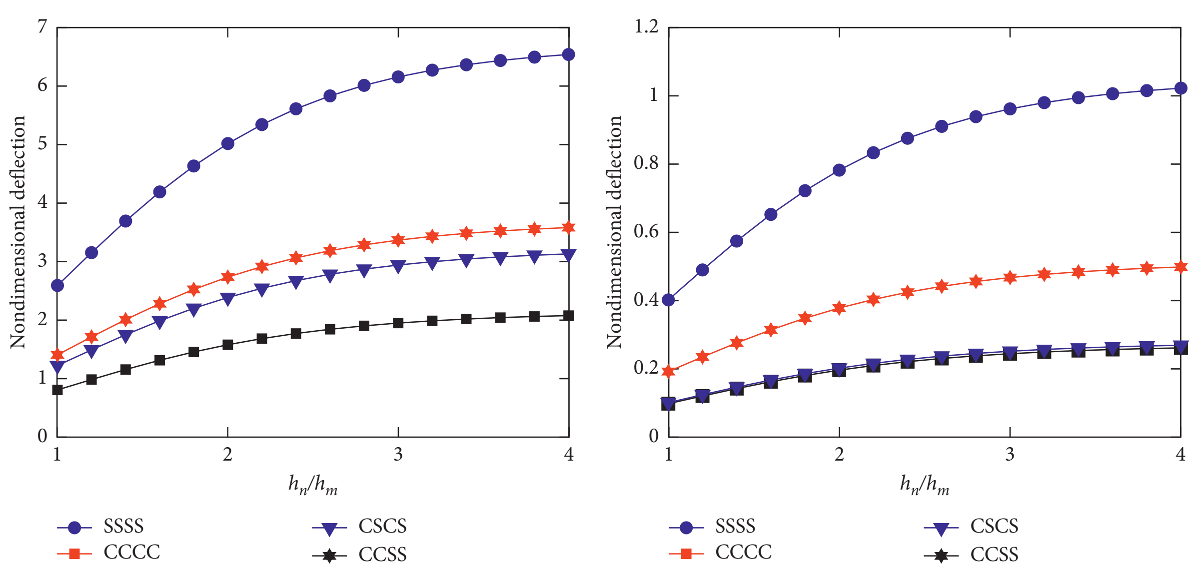


(a) (b)

Figure 5: The effect of ratio $h_n/h_m$ on the nondimensional transverse deflection of the plate with $k_{st}/E_m = 1$: (a) $a/b = 1$; (b) $a/b = 2$.

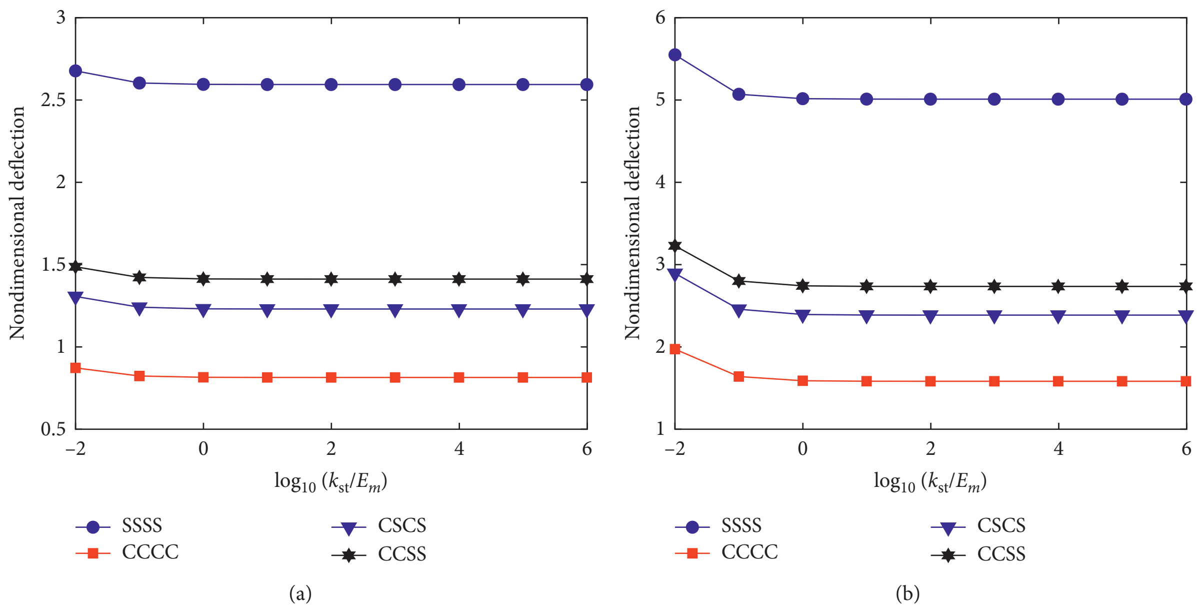


FIGURE 6: The effect of ratio $k_{st}/E_m$ on nondimensional deflection of the plate with $a/b = 1$: (a) $h_n/h_m = 1$; (b) $h_n/h_m = 2$.

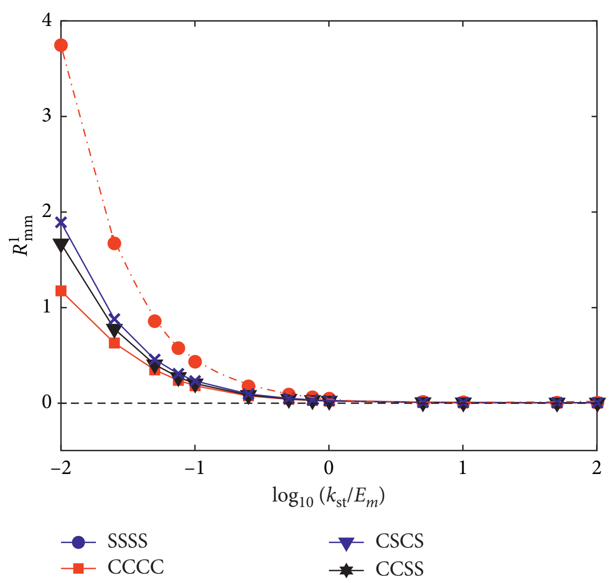


FIGURE 7: The effect of ratio $k_{st}/E_m$ on $R^1_{mn}$ of the plate with $h_n/h_m = 1$.

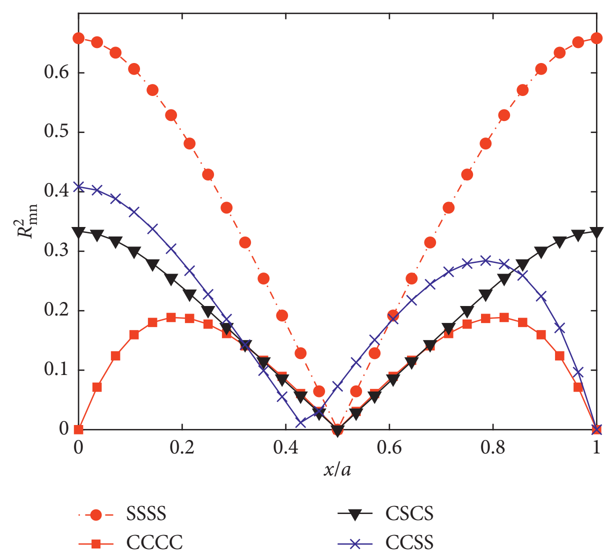


FIGURE 8: The slip between the top and bottom layers at the contact place varying along the $x$-direction, with $k_{st}/E_m = 0.1$ and $h_n/h_m = 1$.

We can see again in Figure 7 that when the stiffness of the stub increases, the slip between two layers decreases and tends to zero. By looking at Figure 8 (the ratio $k_{st}/E_m = 0.1$ is employed), it is very interesting to see that the minimum of slip between two layers at the contact place appears at the central plate with symmetric boundary conditions (CCCC, SSSS, and CSCS). The slip gets a maximum value at the simply supported edge, and this slip strongly depends on the boundary condition.

*(4) Influence of Boundary Condition*. We further study the deflection affected by the boundary condition. A square plate with $h_n/h_m = 1$-2 and $k_{st}/E_m = 0$-1 is considered. Figure 9 shows the displacement at $x = a/2$ and along the $y$ direction in four boundary conditions. The boundary condition has strong effects on the deflection magnitude and deformation shape of the plate. It is shown that the plate with the simple support at all edges has the highest deflection and the one with the fully clamped support has the smallest deflection. The deformation shapes of the SSSS plate, CCCC plate, and CSCS plate are symmetric, while the deformation of the CCSS plate is asymmetric.

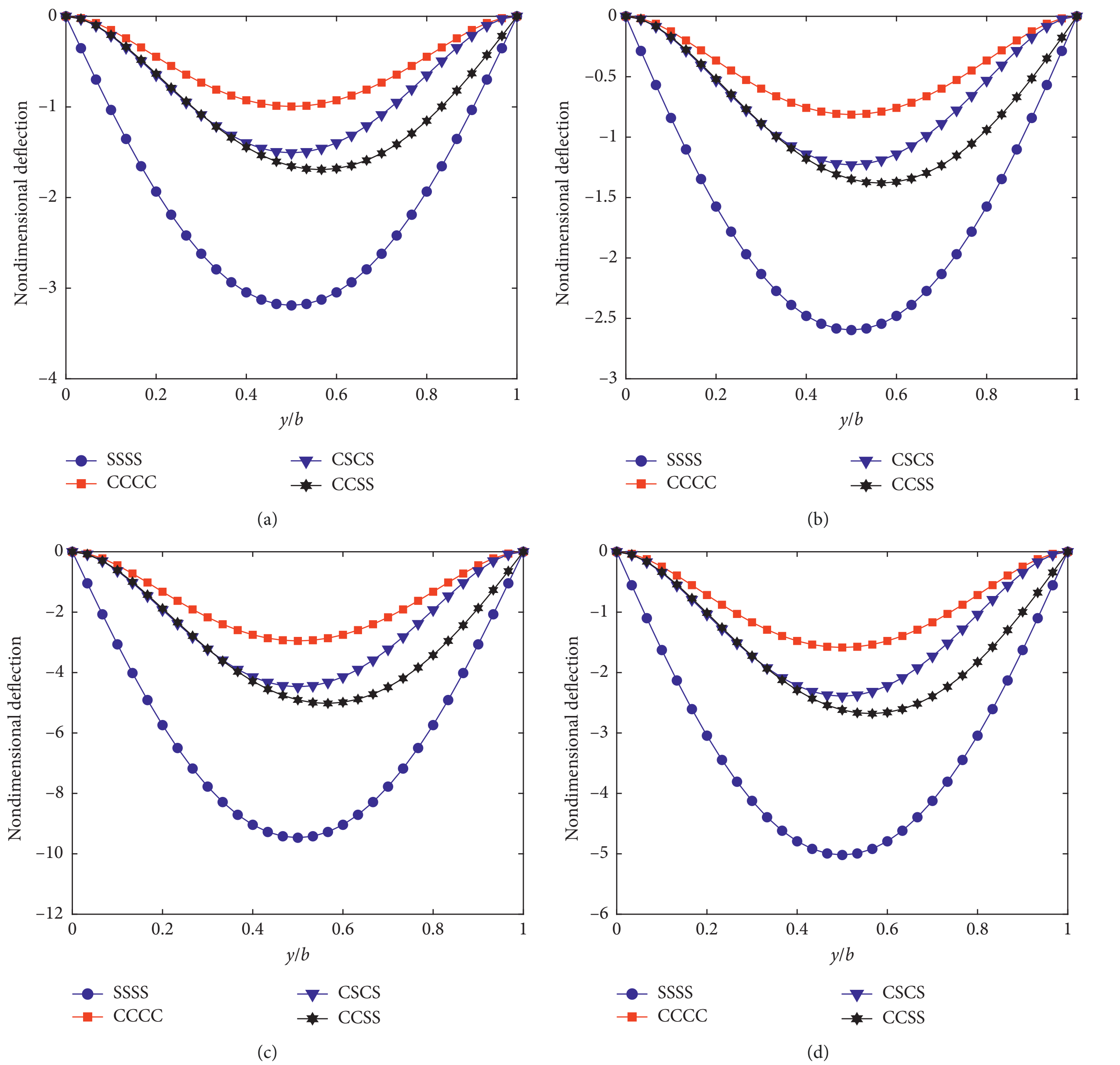


Figure 9: Nondimensional deflection of the plate along the line part $x = a/2$ with $a/b = 1$ and (a) $h_n/h_m = 1$, $k_{st}/E_m = 0$, (b) $h_n/h_m = 1$, $k_{st}/E_m = 1$, (c) $h_n/h_m = 2$, $k_{st}/E_m = 0$, and (d) $h_n/h_m = 2$, $k_{st}/E_m = 1$.

### 3.2. Free Vibration Analysis

*3.2.1. Accuracy Studies.* To confirm the accuracy of this work, we first present a comparison of frequencies of homogeneous CCCC and SSSS plates, with $a = b = 1$ m, $h = a/10$ and $a/100$, $E = 10920$ MPa, and Poisson's ratio $\nu = 0.3$; similar to the bending analysis, $h_n = h_m = 0.5h$ and $k_{st} = 10^{10}E$ are again used for this comparison. The nondimensional frequencies are defined by

$$\overline{\omega}_i = \omega_i a\sqrt{\frac{\rho}{G}}. \tag{65}$$

The results are listed in Tables 6 and 7, in which Ferreira theory [28] was based on FEM and Mindlin theory [28] was based on the analytical solution. As expected, the results obtained by this work match well with those derived from other solutions.

Next, we compare the nondimensional frequencies of an SSSS composite plate 0/90°. The parameters of this plate are set to be $E_1/E_2 = 25$, $G_{12} = G_{13} = 0.5E_2$, $G_{23} = 0.2E_2$, $\nu_{12} = 0.25$, $(a/b) = 1$, and $(a/h) = 10$. The nondimensional frequencies of the plate are normalized by

$$\tilde{\omega}_i = \omega_i\frac{b^2}{\pi^2}\sqrt{\frac{\rho h}{D_{22}}}, \quad (i = 1-6). \tag{66}$$

The comparison is shown in Table 8; note that the results in [29] are obtained from the exact solution. We can see that

Table 6: Comparison of the nondimensional frequencies of an SSSS plate.

| $a/h$ | Mode | Ferreira [28] | Mindlin [28] | Present |
|---|---|---|---|---|
| 10 | 1 | 0.9346 | 0.930 | 0.9271 |
| | 2 | 2.2545 | 2.219 | 2.2055 |
| | 3 | 2.2545 | 2.219 | 2.2055 |
| | 4 | 3.4592 | 3.406 | 3.3600 |
| | 5 | 4.3031 | 4.149 | 4.1123 |
| | 6 | 4.3031 | 4.149 | 4.1123 |
| 100 | 1 | 0.0965 | 0.0963 | 0.0952 |
| | 2 | 0.2430 | 0.2406 | 0.2343 |
| | 3 | 0.2430 | 0.2406 | 0.2343 |
| | 4 | 0.3890 | 0.3847 | 0.3680 |
| | 5 | 0.4928 | 0.4807 | 0.4580 |
| | 6 | 0.4928 | 0.4807 | 0.4580 |

Table 7: Comparison of the nondimensional frequencies of a CCCC plate.

| $a/h$ | Mode | Ferreira [28] | Liew et al. [27] | Present |
|---|---|---|---|---|
| 10 | 1 | 1.5955 | 1.5582 | 1.5710 |
| | 2 | 3.0662 | 3.0182 | 2.9927 |
| | 3 | 3.0662 | 3.0182 | 2.9927 |
| | 4 | 4.2924 | 4.1711 | 4.1829 |
| | 5 | 5.1232 | 5.1218 | 4.9441 |
| | 6 | 5.1730 | 5.1594 | 4.9893 |
| 100 | 1 | 0.1750 | 0.1743 | 0.1683 |
| | 2 | 0.3635 | 0.3576 | 0.3431 |
| | 3 | 0.3635 | 0.3576 | 0.3432 |
| | 4 | 0.5358 | 0.5240 | 0.4978 |
| | 5 | 0.6634 | 0.6465 | 0.6014 |
| | 6 | 0.6665 | 0.6505 | 0.6057 |

Table 8: Comparison of the nondimensional frequencies $\tilde{\omega}_i$ of a square SSSS composite plate.

| Mode | $E_1/E_2 = 10$ | | $E_1/E_2 = 20$ | |
|---|---|---|---|---|
| | Reddy [29] | Present | Reddy [29] | Present |
| 1 | 1.183 | 1.151 | 0.990 | 1.032 |
| 2 | 3.174 | 3.209 | 2.719 | 2.966 |
| 3 | 3.174 | 3.209 | 2.719 | 2.966 |
| 4 | 4.733 | 5.057 | 3.959 | 4.101 |
| 5 | 6.666 | 6.399 | 5.789 | 5.806 |
| 6 | 6.666 | 6.399 | 5.789 | 5.806 |

the present results and reference results are close to each other. From two comparisons, we conclude that the accuracy of this approach is accepted.

*3.2.2. Numerical Results for Free Vibration Analysis of Two-Layer Composite Plates.* In this section, we research the natural frequency of the two-layer composite plate utilizing the proposed method. The two-layer composite plate (length $a$, width $b$, thickness of the top layer $h_n$, and thickness of the bottom layer $h_m$) is studied herein. The nondimensional fundamental frequency is defined as

$$\breve{\omega} = \omega_1 \cdot 100 \cdot a\sqrt{\frac{2(1+\nu_m)\rho}{E_m}}. \quad (67)$$

*(1) Influence of Length-to-Width Ratio.* Table 9 and Figure 10 show the dimensionless fundamental frequencies as a function of aspect ratio $a/b$ with $h_n/h_m = 1$ and $k_{st}/E_m = 1$ of two-layer composite plates altered by the boundary condition. It is evident that the highest and the smallest natural frequencies are found for CCCC and SSSS plates, respectively. When the aspect ratio $a/b$ increases, the nondimensional fundamental frequency increases, and the fundamental frequencies of CCCC and CSCS plates are close when the aspect ratio $a/b > 2.6$; this is a similar behavior to the static bending problem.

*(2) Influence of Thickness-to-Thickness Ratio $h_n/h_m$.* To study the influence of thickness-to-thickness ratio $h_n/h_m$, a two-layer square composite plate with $k_{st}/E_m = 1$ is used for this analysis. The nondimensional fundamental frequencies as a function of the ratio $h_n/h_m$ are tabulated in Table 10 and shown in Figures 11 and 12. The nondimensional fundamental frequency varies nonlinearly with the increasing ratio $h_n/h_m$; the minimum value of fundamental frequency will be obtained when the ratio $h_n/h_m$ is in the range of 1.8 to 2.6.

*(3) Influence of Stiffness of the Connector Stub.* In this exploration, the effect of stiffness of the connector stub on the nondimensional fundamental frequency of the two-layer composite plate is studied. A square two-layer plate with $a/b = 1$ and $k_{st}/E_m$ varying from 0 to $10^6$ is investigated. Table 11 and Figure 13 report the computed results of this plate with $h_n/h_m = 1$; we can see that increasing the ratio $k_{st}/E_m$ from 0 to 1 leads to the increase in the frequencies. When the ratio $(k_{st}/E_m) > 1$, the nondimensional fundamental frequency is almost unchanged.

Figures 14 and 15 plot nondimensional fundamental frequencies of the plate as a function of ratios $a/b$, $h_n/h_m$, and $k_{st}/E_m$. In addition, the first six mode shapes of plates with boundary conditions such as SSSS, CCCC, CSCS, and CCSS are shown in Figures 16–19 with $a/b = 1$, $h_n/h_m = 1$, and $k_{st}/E_m = 10^{-1}$. It is seen that the boundary condition has an effect on mode shapes as well as on the value of frequencies.

Table 9: Influence of ratio $a/b$ on nondimensional fundamental frequency of the plate with $h_n/h_m = 1$ and $k_{st}/E_m = 1$.

| $a/b$ | Boundary | | | |
|---|---|---|---|---|
| | SSSS | CCCC | CSCS | CCSS |
| 0.5 | 0.8439 | 1.6701 | 0.9329 | 1.2115 |
| 1.0 | 1.3505 | 2.4421 | 1.9700 | 1.8434 |
| 1.2 | 1.6474 | 3.0049 | 2.6189 | 2.2592 |
| 1.4 | 1.9983 | 3.7145 | 3.3955 | 2.7687 |
| 1.6 | 2.4029 | 4.5647 | 4.2971 | 3.3698 |
| 1.8 | 2.8614 | 5.5501 | 5.3220 | 4.0606 |
| 2.0 | 3.3737 | 6.6663 | 6.4691 | 4.8395 |
| 2.2 | 3.9398 | 7.9101 | 7.7374 | 5.7053 |
| 2.4 | 4.5595 | 9.2791 | 9.1262 | 6.6570 |
| 2.6 | 5.2330 | 10.7714 | 10.6349 | 7.6938 |
| 2.8 | 5.9601 | 12.3857 | 12.2627 | 8.8151 |
| 3.0 | 6.7408 | 14.1208 | 14.0093 | 10.0203 |
| 3.2 | 7.5751 | 15.9757 | 15.8739 | 11.3092 |
| 3.4 | 8.4628 | 17.9494 | 17.8561 | 12.6811 |
| 3.6 | 9.4040 | 20.0412 | 19.9553 | 14.1359 |
| 3.8 | 10.3985 | 22.2503 | 22.1709 | 15.6730 |
| 4.0 | 11.4463 | 24.5760 | 24.5023 | 17.2922 |

Table 10: Influence of ratio $h_n/h_m$ on nondimensional fundamental frequency of the square plate with $a/b = 1$ and $k_{st}/E_m = 1$.

| $h_n/h_m$ | Boundary | | | |
|---|---|---|---|---|
| | SSSS | CCCC | CSCS | CCSS |
| 1.0 | 1.3505 | 2.4421 | 1.9700 | 1.8434 |
| 1.2 | 1.2757 | 2.3022 | 1.8582 | 1.7396 |
| 1.4 | 1.2231 | 2.2024 | 1.7789 | 1.6661 |
| 1.6 | 1.1872 | 2.1332 | 1.7241 | 1.6156 |
| 1.8 | 1.1641 | 2.0873 | 1.6880 | 1.5825 |
| 2.0 | 1.1506 | 2.0591 | 1.6662 | 1.5627 |
| 2.2 | 1.1445 | 2.0445 | 1.6552 | 1.5530 |
| 2.4 | 1.1439 | 2.0403 | 1.6526 | 1.5511 |
| 2.6 | 1.1476 | 2.0439 | 1.6562 | 1.5550 |
| 2.8 | 1.1544 | 2.0535 | 1.6646 | 1.5633 |
| 3.0 | 1.1635 | 2.0676 | 1.6765 | 1.5749 |
| 3.2 | 1.1744 | 2.0850 | 1.6911 | 1.5889 |
| 3.4 | 1.1866 | 2.1049 | 1.7077 | 1.6048 |
| 3.6 | 1.1997 | 2.1266 | 1.7256 | 1.6219 |
| 3.8 | 1.2133 | 2.1496 | 1.7446 | 1.6399 |
| 4.0 | 1.2274 | 2.1734 | 1.7642 | 1.6585 |

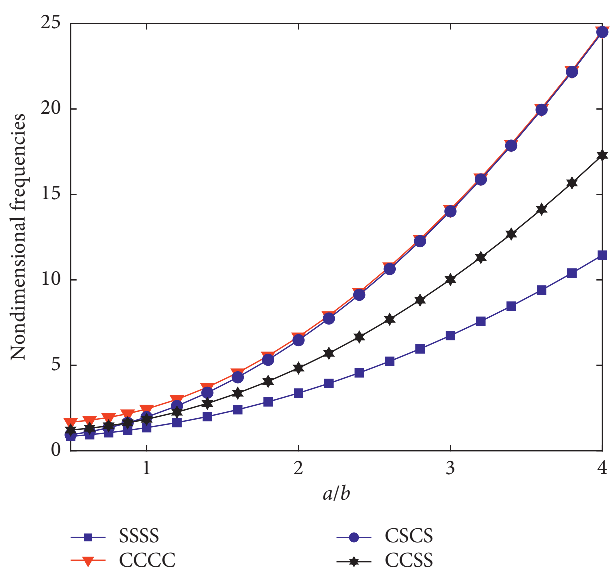


Figure 10: The effect of ratio $a/b$ on nondimensional fundamental frequencies of the plate with $h_n/h_m = 1$ and $k_{st}/E_m = 1$.

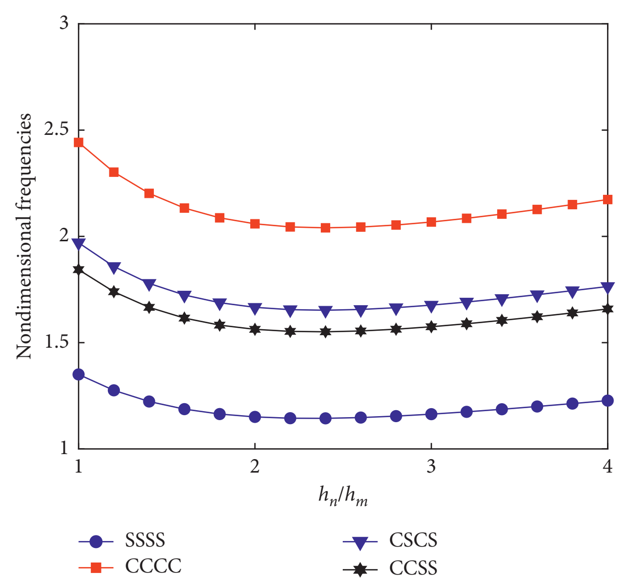


Figure 11: The effect of ratio $h_n/h_m$ on nondimensional fundamental frequencies of the plate with $a/b = 1$ and $k_{st}/E_m = 1$.

## 4. Conclusions

In this work, new numerical results of mechanical behaviors and free vibration responses of the two-layer composite plate are explored, in which two layers are connected by stubs. We used the finite element method combined with the new modified first-order shear deformation theory, which has the following advantages:

(i) Simple formulations for theoretical representation

(ii) No need for reduced integration or selective reduced integration scheme for the proposed method

The computed results of static bending and free vibration obtained by this approach are also compared to other solutions, showing a good agreement. We gained insight into the responses of deflections and natural frequencies. Besides, some geometrical and physical properties of this structure are also examined. Finally, from new numerical results, several conclusions may be achieved as follows:

(i) The stiffness of the stub has a strong effect on static bending deflections and natural frequencies of the two-layer composite plate when $k_{st}/E_m < 1$. When $k_{st}/E_m > 1$, there is no slip between the top and the bottom layers at the contact place, and the static bending and free vibration responses of this plate are similar to those of the one-layer composite plate without stubs.

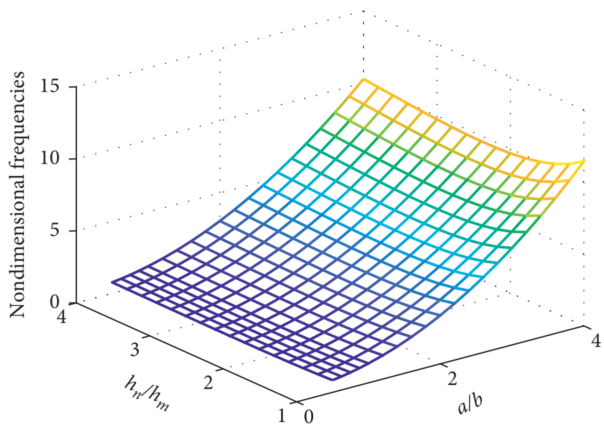


FIGURE 12: Nondimensional fundamental frequencies as a function of $h_n/h_m$ and $a/b$ of the SSSS plate with $k_{st}/E_m = 1$.

TABLE 11: Influence of ratio $k_{st}/E_m$ on nondimensional fundamental frequency of the plate with $a/b = 1$ and $h_n/h_m = 1$.

| $k_{st}/E_m$ | Boundary SSSS | CCCC | CSCS | CCSS |
|---|---|---|---|---|
| 0 | 1.2206 | 2.2205 | 1.7881 | 1.6710 |
| $10^{-2}$ | 1.3292 | 2.3636 | 1.9142 | 1.7976 |
| $10^{-1}$ | 1.3482 | 2.4308 | 1.9625 | 1.8376 |
| $10^{0}$ | 1.3505 | 2.4421 | 1.9700 | 1.8434 |
| $10^{1}$ | 1.3507 | 2.4433 | 1.9708 | 1.8441 |
| $10^{2}$ | 1.3508 | 2.4435 | 1.9709 | 1.8441 |
| $10^{3}$ | 1.3508 | 2.4435 | 1.9709 | 1.8441 |
| $10^{4}$ | 1.3508 | 2.4435 | 1.9709 | 1.8441 |
| $10^{5}$ | 1.3508 | 2.4435 | 1.9709 | 1.8441 |
| $10^{6}$ | 1.3506 | 2.4434 | 1.9710 | 1.8439 |

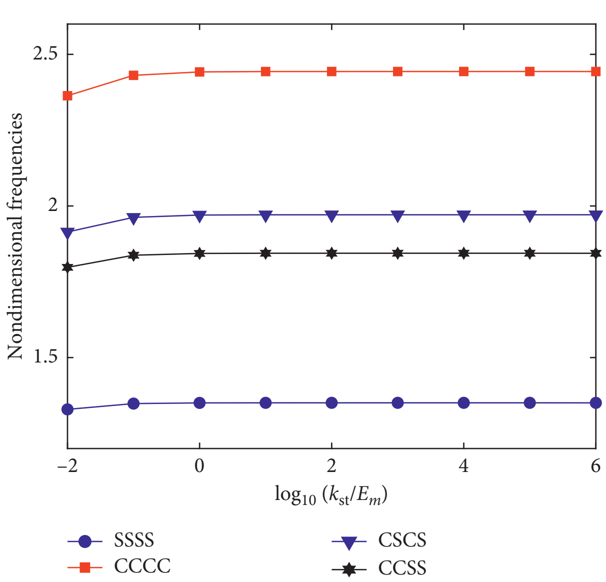


FIGURE 13: The effect of ratio $k_{st}/E_m$ on nondimensional fundamental frequencies of the plate with $a/b = 1$ and $h_n/h_m = 1$.

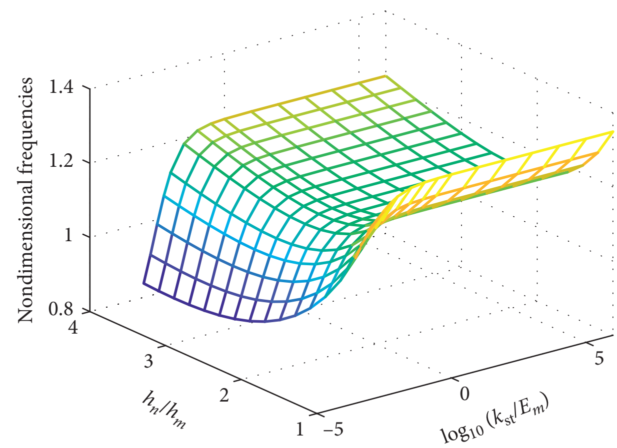


FIGURE 14: Nondimensional fundamental frequencies as a function of $k_{st}/E_m$ and $h_n/h_m$ of the SSSS plate with $a/b = 1$.

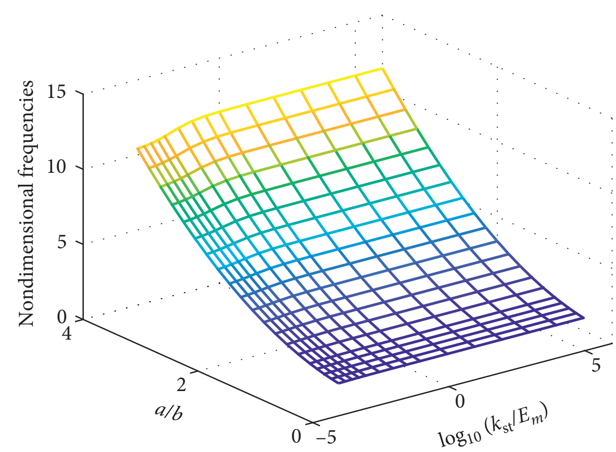


FIGURE 15: Nondimensional fundamental frequencies as a function of $k_{st}/E_m$ and $a/b$ of the SSSS plate with $h_n/h_m = 1$.

(ii) Likewise, the boundary condition has great effect on the slip between two layers, the minimum slip appears at the center of the plates with the symmetric boundary condition, and the slip has the greatest value at the simply supported edge.

(iii) When the ratio $h_n/h_m$ increases, the static bending deflection increases, but the fundamental frequency varies as a nonlinear function of this ratio.

(iv) The higher the ratio $a/b$, the smaller the deflection and the higher the fundamental frequency.

The new results of this work are useful for calculation, design, and testing, as well as for giving the optimal solution for the two-layer plate and shell in engineering and technologies. This study suggests some further works on buckling, dynamic response, and heat transfer problems of the two-layer composite plate using different plate theories.

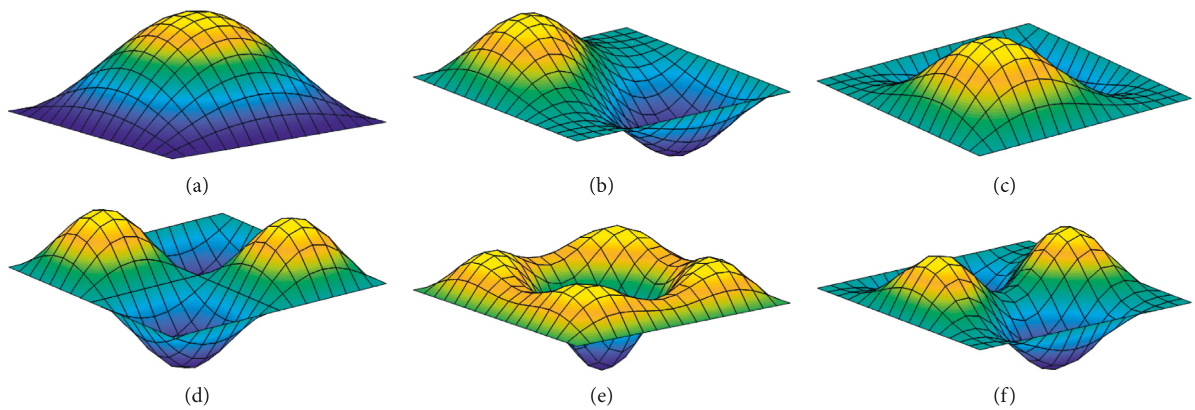

Figure 16: The first six mode shapes of a two-layer square SSSS composite plate. (a) Mode 1. (b) Mode 2. (c) Mode 3. (d) Mode 4. (e) Mode 5. (f) Mode 6.

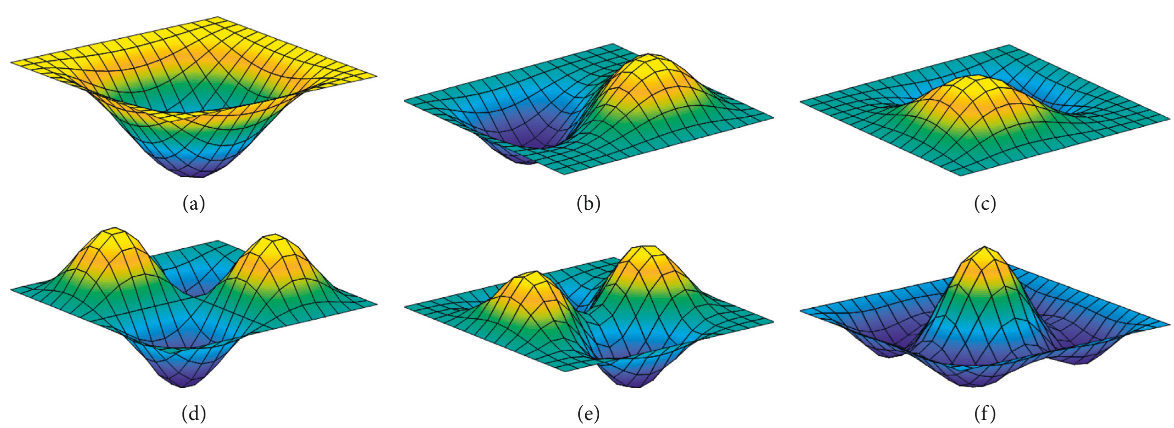

Figure 17: The first six mode shapes of a two-layer square CCCC composite plate. (a) Mode 1. (b) Mode 2. (c) Mode 3. (d) Mode 4. (e) Mode 5. (f) Mode 6.

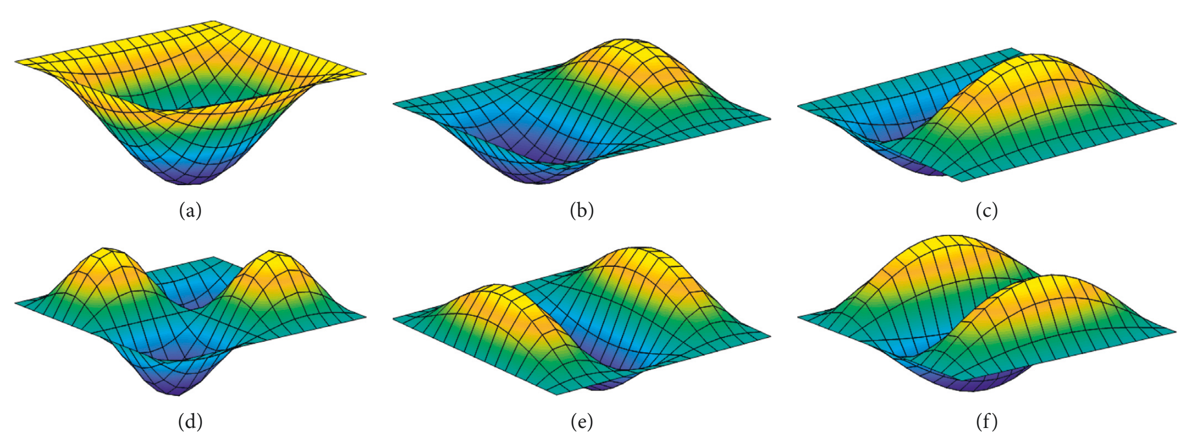

Figure 18: The first six mode shapes of a two-layer square CSCS composite plate. (a) Mode 1. (b) Mode 2. (c) Mode 3. (d) Mode 4. (e) Mode 5. (f) Mode 6.

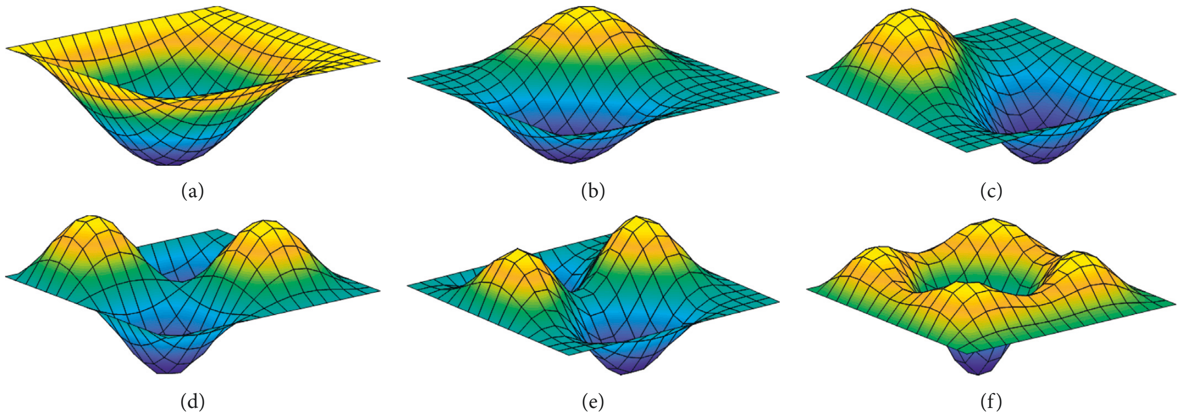

FIGURE 19: The first six mode shapes of a two-layer square CCSS composite plate. (a) Mode 1. (b) Mode 2. (c) Mode 3. (d) Mode 4. (e) Mode 5. (f) Mode 6.

## Appendix

The matrix **C** in equation (30) is defined as

$$
\begin{aligned}
C &= \left[ C_1^T \ C_2^T \ C_3^T \ C_4^T \right]^T, \\
C_1 &= \begin{bmatrix} 1 & -1 & -1 & 1-\frac{8D}{Sa^2} & 1 & 1-\frac{8D}{Sb^2} & \frac{24D}{Sa^2}-1 & \frac{8D}{Sa^2}-1 & \frac{8D}{Sb^2}-1 & \frac{24D}{Sb^2}-1 & 1-\frac{24D}{Sa^2} & 1-\frac{24D}{Sb^2} \\ 0 & -\frac{2}{a} & 0 & \frac{4}{a} & \frac{2}{a} & 0 & -\frac{6}{a} & -\frac{4}{a} & -\frac{2}{a} & 0 & \frac{6}{a} & \frac{2}{a} \\ 0 & 0 & -\frac{2}{b} & 0 & \frac{2}{b} & \frac{4}{b} & 0 & -\frac{2}{b} & -\frac{4}{b} & -\frac{6}{b} & \frac{2}{b} & \frac{6}{b} \end{bmatrix}, \\
C_2 &= \begin{bmatrix} 1 & 1 & -1 & 1-\frac{8D}{Sa^2} & -1 & 1-\frac{8D}{Sb^2} & 1-\frac{24D}{Sa^2} & \frac{8D}{Sa^2}-1 & 1-\frac{8D}{Sb^2} & \frac{24D}{Sb^2}-1 & \frac{24D}{Sa^2}-1 & \frac{24D}{Sb^2}-1 \\ 0 & -\frac{2}{a} & 0 & -\frac{4}{a} & \frac{2}{a} & 0 & -\frac{6}{a} & \frac{4}{a} & -\frac{2}{a} & 0 & \frac{6}{a} & \frac{2}{a} \\ 0 & 0 & -\frac{2}{b} & 0 & -\frac{2}{b} & \frac{4}{b} & 0 & -\frac{2}{b} & \frac{4}{b} & -\frac{6}{b} & -\frac{2}{b} & -\frac{6}{b} \end{bmatrix}, \\
C_3 &= \begin{bmatrix} 1 & 1 & 1 & 1-\frac{8D}{Sa^2} & 1 & 1-\frac{8D}{Sb^2} & 1-\frac{24D}{Sa^2} & 1-\frac{8D}{Sa^2} & 1-\frac{8D}{Sb^2} & 1-\frac{24D}{Sb^2} & 1-\frac{24D}{Sa^2} & 1-\frac{24D}{Sb^2} \\ 0 & -\frac{2}{a} & 0 & -\frac{4}{a} & -\frac{2}{a} & 0 & -\frac{6}{a} & -\frac{4}{a} & -\frac{2}{a} & 0 & -\frac{6}{a} & -\frac{2}{a} \\ 0 & 0 & -\frac{2}{b} & 0 & -\frac{2}{b} & -\frac{4}{b} & 0 & -\frac{2}{b} & -\frac{4}{b} & -\frac{6}{b} & -\frac{2}{b} & -\frac{6}{b} \end{bmatrix}, \\
C_4 &= \begin{bmatrix} 1 & -1 & 1 & 1-\frac{8D}{Sa^2} & -1 & 1-\frac{8D}{Sb^2} & \frac{24D}{Sa^2}-1 & 1-\frac{8D}{Sa^2} & \frac{8D}{Sb^2}-1 & 1-\frac{24D}{Sb^2} & \frac{24D}{Sa^2}-1 & \frac{24D}{Sb^2}-1 \\ 0 & -\frac{2}{a} & 0 & \frac{4}{a} & -\frac{2}{a} & 0 & -\frac{6}{a} & \frac{4}{a} & -\frac{2}{a} & 0 & -\frac{6}{a} & -\frac{2}{a} \\ 0 & 0 & -\frac{2}{b} & 0 & \frac{2}{b} & -\frac{4}{b} & 0 & -\frac{2}{b} & \frac{4}{b} & -\frac{6}{b} & \frac{2}{b} & \frac{6}{b} \end{bmatrix},
\end{aligned} \tag{A.1}
$$

where $D = D_n$ and $S = S_n$ for layer $n$ and $D = D_m$ and $S = S_m$ for layer $m$.

## Data Availability

The data used to support the findings of this study are included within the article.

## Conflicts of Interest

The authors declare that they have no conflicts of interest.

## Acknowledgments

DVT gratefully acknowledges the support of Vietnam National Foundation for Science and Technology Development (NAFOSTED) under Grant no. 107.02-2018.30.

## References

[1] P. Foraboschi, "Behavior and failure strength of laminated glass beams," *Journal of Engineering Mechanics*, vol. 133, no. 12, pp. 1290–1301, 2007.

[2] P. Foraboschi, "Analytical solution of two-layer beam taking into account nonlinear interlayer slip," *Journal of Engineering Mechanics*, vol. 135, no. 10, pp. 1129–1146, 2009.

[3] A. Kryžanowski, S. Schnabl, G. Turk, and I. Planinc, "Exact slip-buckling analysis of two-layer composite columns," *International Journal of Solids and Structures*, vol. 46, no. 14-15, pp. 2929–2938, 2009.

[4] P. L. Grognec, Q. H. Nguyen, and M. Hjiaj, "Exact buckling solution for two-layer Timoshenko beams with interlayer slip," *International Journal of Solids and Structures*, vol. 49, no. 1, pp. 143–150, 2012.

[5] G. He and X. Yang, "Finite element analysis for buckling of two-layer composite beams using Reddy's higher order beam theory," *Finite Elements in Analysis and Design*, vol. 83, pp. 49–57, 2014.

[6] G. He and X. Yang, "Dynamic analysis of two-layer composite beams with partial interaction using a higher order beam theory," *International Journal of Mechanical Sciences*, vol. 90, pp. 102–112, 2015.

[7] G. He, D. Wang, and X. Yang, "Analytical solutions for free vibration and buckling of composite beams using a higher order beam theory," *Acta Mechanica Solida Sinica*, vol. 29, no. 3, pp. 300–315, 2016.

[8] T. Hozjan, M. Saje, S. Srpčič, and I. Planinc, "Geometrically and materially non-linear analysis of planar composite structures with an interlayer slip," *Computers & Structures*, vol. 114-115, pp. 1–17, 2013.

[9] P. Wu, D. Zhou, W. Liu, L. Wan, and D. Liu, "Elasticity solution of two-layer beam with a viscoelastic interlayer considering memory effect," *International Journal of Solids and Structures*, vol. 94-95, pp. 76–86, 2016.

[10] P. Wu, D. Zhou, and W. Liu, "2-D elasticity solutions of two-layer composite beams with an arbitrarily shaped interface," *Applied Mathematical Modelling*, vol. 40, no. 2, pp. 1477–1493, 2016.

[11] M. A. Uddin, A. H. Sheikh, T. Bennett, and B. Uy, "Large deformation analysis of two layered composite beams with partial shear interaction using a higher order beam theory," *International Journal of Mechanical Sciences*, vol. 122, pp. 331–340, 2017.

[12] J. Wen, A. H. Sheikh, M. A. Uddin, and B. Uy, "Analytical model for flexural response of two-layered composite beams with interfacial shear slip using a higher order beam theory," *Composite Structures*, vol. 184, pp. 789–799, 2018.

[13] T. V. Do, T. Q. Bui, T. T. Yu, D. T. Pham, and C. T. Nguyen, "Role of material combination and new results of mechanical behaviour for FG sandwich plates in thermal environment," *Journal of Computational Science*, vol. 21, pp. 164–181, 2017.

[14] B. Cas, I. Planinc, and S. Schnabl, "Analytical solution of three-dimensional two-layer composite beam with interlayer slips," *Engineering Structures*, vol. 173, pp. 269–282, 2018.

[15] K. Ke, M. C. H. Yam, A. C. C. Lam, and K. F. Chung, "Local web buckling of single-coped beam connections with slender web," *Journal of Constructional Steel Research*, vol. 150, pp. 543–555, 2018.

[16] C. T. Latham, A. Toledano, H. Murakami, and F. Seible, "A shear-deformable two-layer plate element with interlayer slip," *International Journal for Numerical Methods in Engineering*, vol. 26, no. 8, pp. 1769–1789, 1988.

[17] P. Foraboschi, "Analytical model for laminated-glass plate," *Composites Part B: Engineering*, vol. 43, no. 5, pp. 2094–2106, 2012.

[18] D. Baraldi, A. Cecchi, and P. Foraboschi, "Broken tempered laminated glass: non-linear discrete element modeling," *Composite Structures*, vol. 140, pp. 278–295, 2016.

[19] P. Foraboschi, "Layered plate with discontinuous connection: exact mathematical model," *Composites Part B: Engineering*, vol. 47, pp. 365–378, 2013.

[20] P. Foraboschi, "Three-layered sandwich plate: exact mathematical model," *Composites Part B: Engineering*, vol. 45, no. 1, pp. 1601–1612, 2013.

[21] P. Foraboschi, "Three-layered plate: elasticity solution," *Composites Part B: Engineering*, vol. 60, pp. 764–776, 2014.

[22] P. Wu, D. Zhou, W. Liu, W. Lu, and H. Fang, "3-D exact solution of two-layer plate bonded by a viscoelastic interlayer with memory effect," *Composite Structures*, vol. 164, pp. 291–303, 2017.

[23] P. Vidal, L. Gallimard, and O. Polit, "Robust layerwise C 0 finite element approach based on a variable separation method for the modeling of composite and sandwich plates," *Finite Elements in Analysis and Design*, vol. 139, pp. 1–13, 2018.

[24] M. M. Alinia, G. Soltanieh, and M. Amani, "Inelastic buckling behavior of stocky plates under interactive shear and in-plane bending," *Thin-Walled Structures*, vol. 55, pp. 76–84, 2012.

[25] I. Senjanović, N. Vladimir, and N. Hadžić, "Modified Mindlin plate theory and shear locking-free finite element formulation," *Mechanics Research Communications*, vol. 55, pp. 95–104, 2014.

[26] H.-T. Thai and D.-H. Choi, "A simple first-order shear deformation theory for laminated composite plates," *Composite Structures*, vol. 106, pp. 754–763, 2013.

[27] K. M. Liew, J. Wang, T. Y. Ng, and M. J. Tan, "Free vibration and buckling analyses of shear-deformable plates based on FSDT meshfree method," *Journal of Sound and Vibration*, vol. 276, no. 3–5, pp. 997–1017, 2004.

[28] A. J. M. Ferreira, *MATLAB Codes for Finite Element Analysis: Solids and Structures*, Springer, Dordrecht, Netherlands, 2009, ISBN 9789400789555.

[29] J. N. Reddy, *Mechanics of Laminated Composite Plates and Shells: Theory and Analysis*, CRC Press, Boca Raton, FL, USA, 2003. ISBN 9780849315923.